ACS OMEGA

http://pubs.acs.org/journal/acsodf

Article

Nanoarchitectonic E-Tongue of Electrospun Zein/Curcumin Carbon Dots for Detecting *Staphylococcus aureus*in Milk

Andrey Coatrini Soares,[▽] Juliana Coatrini Soares,[▽] Danilo Martins dos Santos, Fernanda L. Migliorini, Mario Popolin-Neto, Danielle dos Santos Cinelli Pinto, Wanessa Araújo Carvalho, Humberto Mello Brandão, Fernando Vieira Paulovich, Daniel Souza Correa, Osvaldo N. Oliveira, Jr,* and Luiz Henrique Capparelli Mattoso*

Cite This: *ACS Omega* 2023, 8, 13721−13732

Read Online

ACCESS | Metrics & More | Article Recommendations | Supporting Information

ABSTRACT: We report a nanoarchitectonic electronic tongue made with flexible electrodes coated with curcumin carbon dots and zein electrospun nanofibers, which could detect *Staphylococcus aureus*(*S. aureus*) in milk using electrical impedance spectroscopy. Electronic tongues are based on the global selectivity concept in which the electrical responses of distinct sensing units are combined to provide a unique pattern, which in this case allowed the detection of *S. aureus* through non-specific interactions. The electronic tongue used here comprised 3 sensors with electrodes coated with zein nanofibers, carbon dots, and carbon dots with zein nanofibers. The capacitance data obtained with the three sensors were processed with a multidimensional projection technique referred to as interactive document mapping (IDMAP) and analyzed using the machine learning-based concept of multidimensional calibration space (MCS). The concentration of *S. aureus* could be determined with the sensing units, especially with the one containing zein as the limit of detection was 0.83 CFU/mL (CFU stands for colony-forming unit). This high sensitivity is attributed to molecular-level interactions between the protein zein and C−H groups in *S. aureus* according to polarization-modulated infrared reflection-absorption spectroscopy (PM-IRRAS) data. Using machine learning and IDMAP, we demonstrated the selectivity of the electronic tongue in distinguishing milk samples from mastitis-infected cows from milk collected from healthy cows, and from milk spiked with possible interferents. Calibration of the electronic tongue can also be reached with the MCS concept employing decision tree algorithms, with an 80.1% accuracy in the diagnosis of mastitis. The low-cost electronic tongue presented here may be exploited in diagnosing mastitis at early stages, with tests performed in the farms without requiring specialized laboratories or personnel.

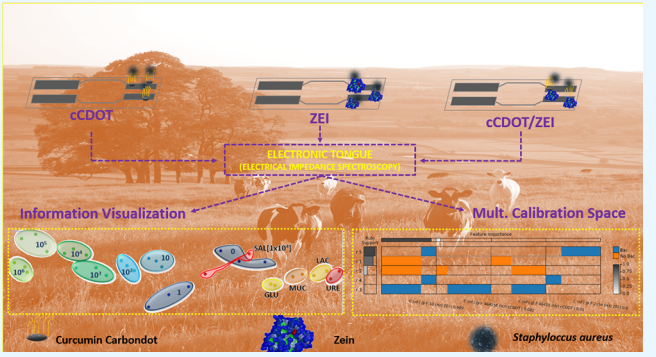

1. INTRODUCTION

The early and fast diagnosis of bovine mastitis caused by infections from microorganisms is crucial to reduce the negative economic impact on the dairy industry owing to milk production reduction with cattle death and reduced milk quality.[1−5] This diagnosis can be made by detecting *Staphylococcus aureus*(*S. aureus*), the prevalent pathogens causing mammary infections in dairy cows[2,5] associated with various forms of clinical and subclinical mastitis.[2] These bacteria are lodged into the mammary glands, which become chronically infected for a few months, serving as a reservoir for new infections in other animals. As a consequence, enzymes and toxins are produced, thus damaging breast tissue and reducing milk production. The cows can be treated with antibiotics, but this should be done at early stages of the disease to guarantee treatment efficiency and decrease of bacteria resistance, as it has happened with the antibiotic methicillin.[1,3] The bacterial isolation and its biochemical characterization[6] or its identification by polymerase chain reaction[6] are two gold standard methods to detect *S. aureus* (and bovine mastitis). The first is time-consuming and laborious, while the second is expensive and requires specialized equipment and trained personnel. Since the gold-standard methods are not amenable for point-of-attention diagnosis, considerable efforts have been made to develop alternative methodologies. The latter include assays to determine the somatic cell count (SCC) in the California Milk Coagulation Test and colorimetric and fluorimetric assays to measure enzyme concentrations in milk.[3,7] Also to be

Received: December 13, 2022
Accepted: March 22, 2023
Published: April 4, 2023

mentioned are the immunosensors to detect *S. aureus*[8−17] and the recent work with an electronic tongue based on impedance spectroscopy.[18]

The advantages of electronic tongues are mostly related to the use of the global selectivity concept, which does not require specific sensors.[19,20] Hence, sensing units more robust than the biosensors can be utilized, whose electrical responses are combined to establish a pattern that is specific − as in a "finger print" − for the liquid under analysis. Electronic tongues are highly sensitive due to interface effects on the sensing units as they are exposed to the liquid samples;[21−23] because these effects are highly dependent on the liquid composition and on the materials of the sensing units, a combination of different responses affords the establishment of this specific pattern.[24] In addition, the electronic tongue developed in this work has other advantages over other devices in the literature, especially potentiometric e-tongues.[25,26] The first novelty is the combination of curcumin and zein fibers in nanoarchitectures, which allowed the development of a flexible device. Such a device can be implanted at a lower cost and with competitive sensitivity with electronic tongues in the literature.[18] It is also significant that the electronic tongue used here does not require reference electrodes and counter-electrodes.

In this paper, we extend the work reported in ref 18 using an nanoarchitectonic electronic tongue made with flexible sensing units that can be produced at a low cost using a 3D cut printer. The sensor array contains curcumin carbon dots and the protein zein, yielding a low-cost device cheaper than biosensors based on specific interaction. Zein, in particular, proved excellent to enhance the electronic tongue performance. The accuracy in *S. aureus*/mastitis detection was evaluated in contaminated milk samples using the information visualization technique referred to as interactive document mapping (IDMAP)[27,28] and the multidimensional calibration space (MCS) concept using machine learning.[29]

2. MATERIALS AND METHODS

2.1. Curcumin Carbon Dots Synthesis and Characterization. Curcumin carbon dots (cCDOT) were synthesized using a slightly modified methodology to that of Ting and colleagues.[30] Curcumin (CCM; 0.30 g) (Sigma-Aldrich, USA) and citric acid (0.60 g) (Sigma-Aldrich, USA) were ground uniformly, suspended in 15 mL of deionized water, and hydrothermally treated in a Teflon-lined autoclave at 180 °C for 1.5 h. This reaction medium was cooled down to room temperature and centrifuged at 10.000 rpm for 15 min. The supernatant was then filtered through a 0.22 μm syringe filter and dialyzed against deionized water using a membrane with nominal molecular weight cutoffs of 2000 Da for 48 h. The resulting cCDOT suspension was then stored at 8 °C until use. The concentration of cCDOT was determined by freeze-drying a suspension aliquot at −45 °C for 48 h (Liotop L101, Liobrás), resulting in a concentration of 1.2 ± 0.1 mg of cCDOT/g suspension. Transmission electron microscopy (TEM) and high-resolution TEM images of cCDOT were obtained with a transmission JEOL JEM2100 LaB6 microscope. Fluorescence spectra were recorded on a Shimadzu (RF-5301PC) spectrofluorimeter using a quartz cuvette. The UV−vis absorption spectra of carbon dot suspensions were acquired with a Shimadzu (UV-1900) spectrophotometer in the range between 200 and 700 nm.

2.2. Electrode Fabrication. Disposable electrodes were prepared with a simple, low-cost cut-printing method as described in ref 31. A conductive ink made of graphite and carbon black powders (90/10 w/w) (Synth, Brazil) suspended in shellac (Acrilex, Brazil) in a proportion of 30% (w/w) was homogeneously deposited onto the adhesive paper and then dried in an air-circulating oven for 1 h at 40 °C.A mask with electrodes, with 12.9 mm^2, containing 1 pair of fingers (spaced by 1.6 mm), was cut from the conductive sheets using a cut printer (Silhouette, model 3, Moema/SP, Brazil) (see Figure S1 in the Supporting Information). Then, the sensors were obtained by removing the mask and adhering them to flexible and waterproof crystal acetate sheets (Artigianato A4, Brazil). The electrospinning method was used to functionalize the electrode. A 300 mg mL^{-1} zein (Sigma-Aldrich, USA) solution in acetic acid (Sigma-Aldrich, USA) was diluted with cCDOT aqueous suspension to obtain a concentration of 240 and 0.24 mg mL^{-1} of zein and cCDOT, respectively. The electrospun solution was transferred to a 3 mL syringe coupled to a syringe pump (New Era, USA), which delivered the solution through a 27-gauge metallic needle (0.45 mm diameter) at a constant flow rate (10 μL/min). Electrospinning was performed for 10 min at a working distance of 8 cm, applied voltage of 22 kV at 25 ± 3 °C, and relative humidity of 30%. Fibers were directly electrospun over the electrode partially covered with aluminum foil and attached to a stainless-steel drum collector, according to Dos Santos et al.[31] The modified electrodes were removed from the aluminum foil and stored in a desiccator before further use.

2.3. Electrode Morphological Characterization. The morphology of electrodes and deposited nanofibers was evaluated by scanning electron microscope (SEM, JEOL 6510) using an acceleration voltage of 10 kV after sputter coating the samples with gold. ImageJ 1.45 software (National Institutes of Health, Bethesda, MD, USA) was used to measure the fiber diameter, whose average value was determined from at least 100 fibers chosen randomly.

***S. aureus*/Mastitis Detection.** The analytical performance of the electronic tongue was assessed using electrical impedance data from three sets of experiments carried out with a Solartron, model 1260 A, in the frequency range from $1-10^6$ Hz, with a DC potential of 0 mV and AC potential of 50 mV. All the experiments were made inside a class II-type B2 biosafety cabinet (Pachane, Brazil) for protection against external contamination. Flexible electrodes were immersed into 50 μL of milk collected from a healthy cow without mastitis − after three negative microbiological tests at 1 week intervals − and spiked with various *S. aureus* (INCQS 00015 ATCC 25923) concentrations (viz., 1, 10, 10^2, 10^3, 10^4, 10^5, and 10^6 CFU/mL) followed by washing with ultrapure water. The milk used in the detection is of the processed type. This milk sample was manually contaminated with the *S. aureus* bacteria, at the concentrations indicated. The samples before spiking with *S. aureus* will be referred to as "blank" milk or control. Impedance spectra were obtained for the latter milk samples, in addition to blank milk samples contaminated with the interferents (see Figure S2 in the Supporting Information) glucose (GLU) (Sigma Aldrich, USA), lactose (Sigma Aldrich, USA) (LAC), urea (Sigma Aldrich, USA) (URE), mucin (Sigma Aldrich, USA) (MUC), and *Salmonella* (SAL[1×10^4] and SAL[1×10^8]) to verify the electronic tongue selectivity. Also used were milk samples collected from five dairy cows, four of which were naturally infected with mastitis and another

https://doi.org/10.1021/acsomega.2c07944
ACS Omega 2023, 8, 13721−13732

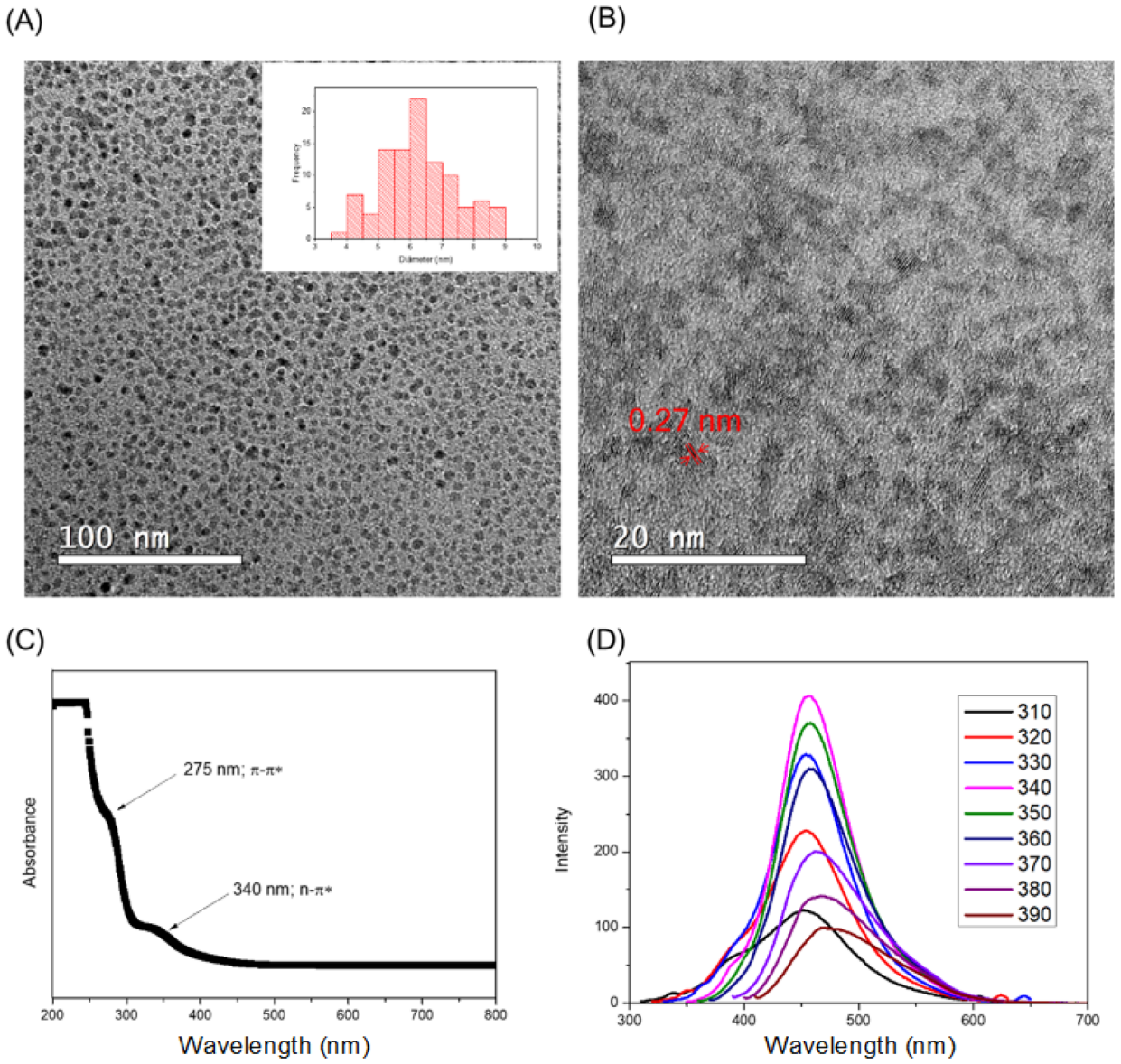

Figure 1. (A) TEM image and histogram for size distribution of cCDOT, (B) high-resolution TEM image of cCDOT with the in-plane lattice spacing, and (C) UV−vis absorption spectra of cCDOT; (D) fluorescence emission spectra of cCDOT at distinct excitation wavelengths.

one was a healthy cow from Embrapa Gado de Leite (Juiz de Fora, MG, Brazil) and Luiz de Queiroz College of Agriculture (ESALQ) (Piracicaba, SP, Brazil) farms. The *S. aureus* mastitis identification was made according to Oliver et al.[6] The milk samples from these cows were subdivided into eleven classes:

1) Milk from a healthy cow (Control) (Animal 1 from Embrapa Gado de Leite);
2) Milk from the left front mammary quarter (left udder) of an infected cow (AE-D0×) (Animal 2 from Embrapa Gado de Leite);
3) Milk from the left front mammary quarter (left udder) of the latter infected cow, diluted 10× (AE D10×) (Animal 2 from Embrapa Gado de Leite);
4) Milk from the left front mammary quarter (left udder) of the latter infected cow, diluted 25× (AE D25×) (Animal 2 from Embrapa Gado de Leite);
5) Milk from the left front mammary quarter (left udder) of the latter infected cow, diluted 50× (AE D50×) - (Animal 2 from Embrapa Gado de Leite);
6) Milk from the right front mammary quarter (right udder) of another infected cow (AD-D0×) (Animal 3 from Embrapa Gado de Leite);
7) Milk from the right front mammary quarter (right udder) of the latter infected cow, diluted 10× (AD D10×) (Animal 3 from Embrapa Gado de Leite);
8) Milk from the right front mammary quarter (right udder) of the latter infected cow, diluted 25× (AD D25×) (Animal 3 from Embrapa Gado de Leite);
9) Milk from the right front mammary quarter (right udder) of the latter infected cow, diluted 50× (AD D50×) (Animal 3 from Embrapa Gado de Leite);
10) Milk from the left front mammary quarter (left udder) of an infected cow, conditioned with bronopol (Sigma-Aldrich, USA, Mw = 199.99 g/mol), with a small somatic cell count (Low SCC) (Animal 4 from Luiz de Queiroz College of Agriculture);
11) Milk from left front mammary quarter (left udder) of another infected cow, conditioned with bronopol, with a

https://doi.org/10.1021/acsomega.2c07944
ACS Omega 2023, 8, 13721−13732

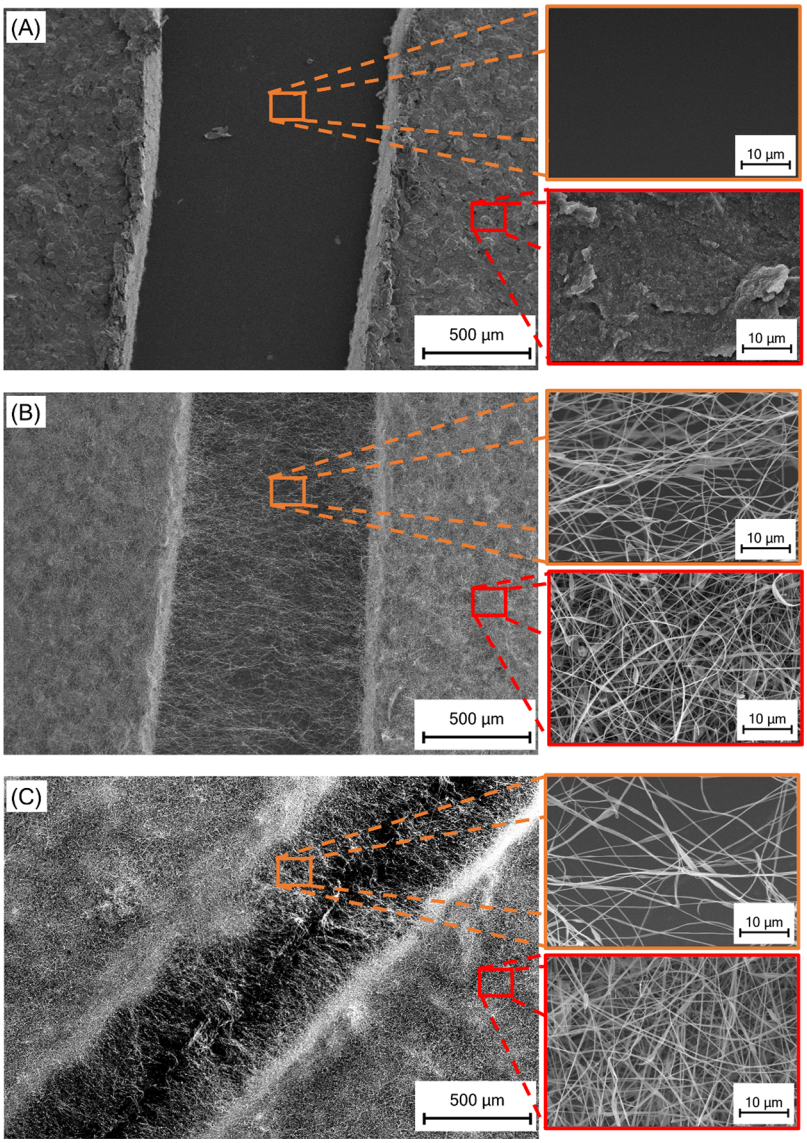

Figure 2. SEM images of the non-modified electrode (A); ZEI/cCdot fibers deposited onto the electrode (B); ZEI fibers deposited onto the electrode (C).

high count of somatic cells (High SCC) (Animal 5 from Luiz de Queiroz College of Agriculture).

The milk composition and somatic cell count were performed on Bentley Combi System 2300 electronic equipment (see the Supporting Information).

2.5. Information Visualization and Machine Learning Techniques for Electronic Tongue Calibration. Dimensionality reduction of electrical impedance data is used to evaluate selectivity and false positive presence.[32] The electrical impedance data were analyzed with the Interactive Document Mapping (IDMAP)[27,28] projection technique to evaluate selectivity and possible existence of false positives. IDMAP considers Euclidean distances in the original space $\delta(x_i, x_j)$ between different class samples $X = \{x_1, x_2, ..., x_n\}$ and projects this data into a lower-dimension 2D space where $Y = \{y_1, y_2, ..., y_n\}$ gives the position of visual elements (or points) representing the samples based on Euclidean distances $d(y_i - y_j)$ in this new 2D visual space. These projections are calculated using eq 1, where δ_{max} and δ_{min} are the maximum and minimum distances between data instances samples and $d(y_i - y_j)$ is the Euclidean distance between points in the visual space.

$$\text{ErrorIDMAP} = \frac{\delta(x_i, x_j) - \delta_{min}}{\delta_{max} - \delta_{min}} - d(y_i - y_j) \quad (1)$$

The Parallel Coordinates[33] technique was applied to the capacitance spectra from blank milk − obtained from a healthy cow without mastitis − contaminated deliberately with *S. aureus* to identify frequencies at which there is a high distinction power to build calibration curves and determine analytical parameters, namely, limit of detection (LoD) and limit of quantification (LoQ). The distinction ability in each frequency was calculated using the silhouette coefficient (S) defined in eq 2, where n is the number of samples, b_i is the minimum average Euclidean distances computed between the ith data point sample and each group of data point samples with different concentrations,[28,33,34] and a_i is the average of the calculated Euclidean distances between the ith data point

https://doi.org/10.1021/acsomega.2c07944
ACS Omega 2023, 8, 13721−13732

sample and the data points of all the samples with the same concentration.

$$S = \frac{1}{n}\sum_{i=1}^{n}\frac{(b_i - a_i)}{\max(b_i, a_i)} \quad (2)$$

For a robust analysis, calibration of the electronic tongue was performed using a machine learning classification model.[35,36] The Multidimensional Calibration Space (MCS) method[29] provides predictability and explainability in classifying samples. From the impedance spectra measured with three sensing units of the electronic tongue, whose molecular architectures are cCDOT/ZEI, cCDOT, and ZEI, we obtained capacitance values at 19 frequencies (1 to 10^6 Hz), resulting in 57 frequencies with the 3 sensors combined. Decision tree (DT)[35−37] models were used for creating the MCS represented visually using ExMatrix,[38] supporting interpretability of the classification task. The Nested KFold Cross-Validation was conducted[39,40] for obtaining DT's hyperparameter combinations and performance estimation. The nested procedure − instead of a single KFold Cross-Validation[36] − can avoid optimistic (overestimation) and biased performance, which are typical issues on small datasets.[39,40]

3. RESULTS AND DISCUSSION

3.1. Curcumin Carbon Dots and Electrode Characterization. Electrodes modified with cCDOT were characterized through microscopic and spectroscopic techniques. TEM images and corresponding size distribution histogram in Figure 1A indicate that cCDOTs have a quasi-spherical morphology and average size of 6.3 ± 1.2 nm. The crystalline nature of cCDOT is revealed in the high-resolution TEM image in Figure 1B with an interlattice distance of 0.27 nm, which corresponds to the diffraction planes (102) of the sp^2 graphitic carbon structure.[30,31] The UV−vis absorption spectrum in Figure 1C for cCDOTs features bands at 275 nm assigned to $\pi \rightarrow \pi^*$ transition of C═C (sp2 aromatic domains) and at 340 nm due to $n \rightarrow \pi^*$ transition of C═O and C−O $n \rightarrow \pi^*$ transition of C═O and C−O.[31] The maximum emission for these cCDOTs occurs at 460 nm under an excitation wavelength of 340 nm in Figure 1D.

Figure 2 shows that the non-modified electrodes exhibit heterogeneous, rough, and lamella-like surfaces. After being coated by electrospinning, the electrode surface and the region between electrodes were covered by a layer of nanofibers with average diameters of 343 ± 105 and 384 ± 114 nm for ZEI and ZEI/cCDOT films, respectively. The incorporation of cCDOTs into zein nanofibers had no significant effect on fiber diameter ($p > 0.05$).

***S. aureus* Detection.** Three film architectures built within the paradigm of nanoarchitectonics from curcumin carbon dots (cCDOT), zein (ZEI), and curcumin carbon dots/zein (cCDOT/ZEI) were employed in the electronic tongue to detect mastitis using electrical impedance spectroscopy. Figure 3 shows the capacitance spectra for *S. aureus* detection in blank milk for the three sensing units. A clear distinction of the *S. aureus* concentrations is observed at low frequencies, below 100 Hz, where the electrical response is governed by the double layer[41,42] that is altered due to non-specific interaction between the film-containing molecules and *S. aureus* in contaminated milk. Distinction of the different samples is more efficient in sensing units comprising zein, thus indicating

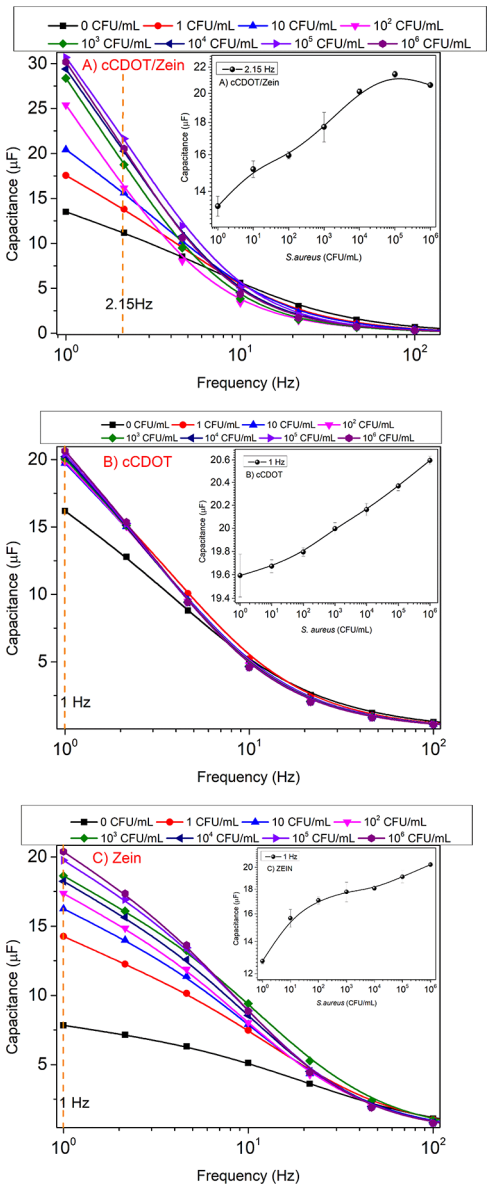

Figure 3. Capacitance spectra for sensing units made with (A) cCDOT/ZEI, (B) cCDOT, and (C) ZEI films used in the e-tongue for detecting *S. aureus*. The insets represent the calibration curves at (A) 2.15 Hz, (B) 1 Hz, and (C) 1 Hz, where the error bars represent standard deviations for each point of the calibration curves.

that this protein can improve selectivity. The calibration curves for the three sensing units are shown in the insets. The *S. aureus* concentration dependence is best represented by plotting the change in the real (C') component of capacitance, which increases at low concentrations before saturation. The limit of detection (LoD) and limit of quantification (LoQ) for each molecular architectures was determined using the International Union of Pure and Applied Chemistry method (IUPAC)[43] from eqs 3 and 4

$$\text{LoD} = \frac{3 \times \text{SD}}{\text{slope}} \quad (3)$$

$$\text{LoQ} = \frac{10 \times \text{SD}}{\text{slope}} \quad (4)$$

https://doi.org/10.1021/acsomega.2c07944
ACS Omega 2023, 8, 13721−13732

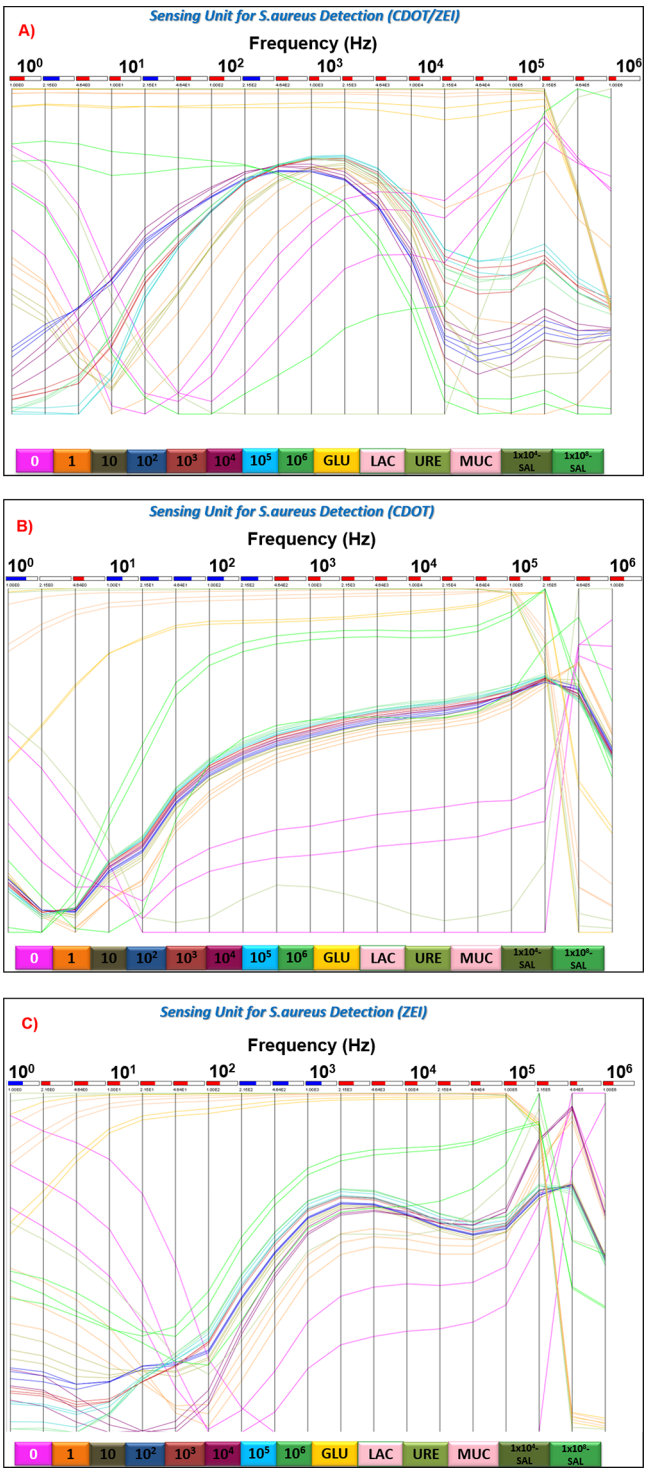

Figure 4. Parallel Coordinates projection of the capacitance spectra using sensing units with molecular architectures cCDOT/ZEI (A), cCDOT (B), and ZEI (C). The spectra were taken with milk samples containing different *S. aureus* concentrations, and interferents GLU, LAC, URE, MUC, and SAL (1×10^4 and 1×10^8 CFU/mL).

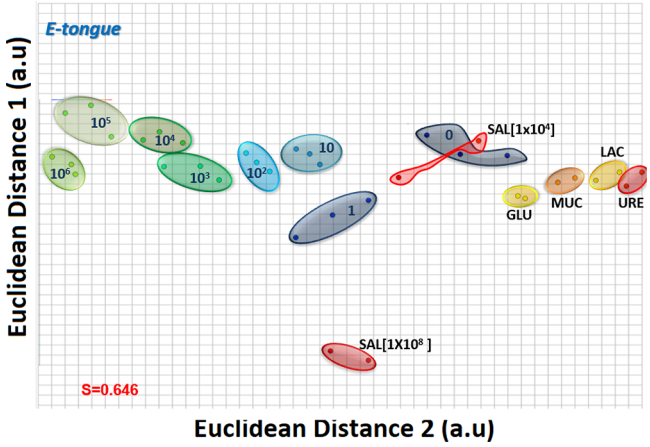

Figure 5. IDMAP plot for the capacitance spectra for *S. aureus* detection in milk samples. The measurements were taken with the electronic tongue comprising 3 sensing units functionalized with cCDOT/ZEI, cCDOT, and ZEI. Note that points related to the interferents glucose (GLU), mucin (MUC), lactose (LAC), urea (URE), and *Salmonella* (SAL[1×10^4] and SAL[1×10^8] CFU/mL) are next to control samples, indicating no false positives.

where SD is the standard deviation in the curves for blank samples, and 3 and 10 are constants chosen according to the confidence level. LoDs for cCDOT, ZEI, and cCDOT/ZEI were, respectively, 4.19, 0.86, and 1.74 CFU/mL, while LoQs were 13.84, 2.83, and 5.76 CFU/mL, respectively. According to McKinnon et al.,[44] dairy cattle infected with mastitis can secrete ~10^7 CFU/mL, indicating that this electronic tongue is capable of detecting *S. aureus* traces both in milk samples from animals contaminated by mastitis and in food quality control. The nanoarchitectures in this electronic tongue are competitive with most devices in the literature,[8−18] especially the one containing ZEI. These details are summarized in Table S1 in the Supporting Information.

The choice of 2.15, 1, and 1 Hz as the frequencies for the calibration curves was based on a study using the parallel coordinates technique[33] to treat the capacitance data, as in the plots in Figure 4. The blue boxes indicate that the corresponding capacitances at that particular frequency are distinct from each other. White boxes refer to frequencies that do not assist in distinguishing the samples, while red boxes refer to frequencies whose use is actually deleterious to the distinction.[45] The blue boxes are located at low frequencies for the three sensing units, as expected with the electrical response being governed by the double layer.

Using IDMAP[27,28] to project the capacitance data from the three sensing units of the electronic tongue, it is possible to distinguish the milk samples contaminated with different *S. aureus* concentrations from those with interferents added to milk. Figure 5 shows the *S. aureus* samples placed progressively farther from the control sample (0 CFU/mL), and the interferent samples (*Salmonella*, glucose, mucin, urease, and lactose) are placed next to 0 CFU/mL. This selectivity could be estimated by calculating the silhouette coefficient (S), which quantifies cohesion and separation between cluster instances. S varies between −1 and +1, where ($S \sim 1$) indicates that the clusters are distinct from each other, with high selectivity; ($S \sim 0$) corresponds to neutral distinction of the clusters, and ($S \sim -1$) shows deleterious cluster distinction and low selectivity.[27,28] For the electronic tongue, the silhouette coefficient was 0.646, which may be considered as selective.[27,28] In subsidiary analyses, we noted that each single sensing unit can separately distinguish the *S. aureus* samples (Figure S3 in the Supporting Information) with silhouette coefficients 0.573, 0.631, and 0.561 for cCDOT/ZEI, cCDOT, and ZEI, respectively.

3.3. Calibration of the Electronic Tongue Using Machine Learning. One of the major challenges in the

https://doi.org/10.1021/acsomega.2c07944
ACS Omega 2023, 8, 13721−13732

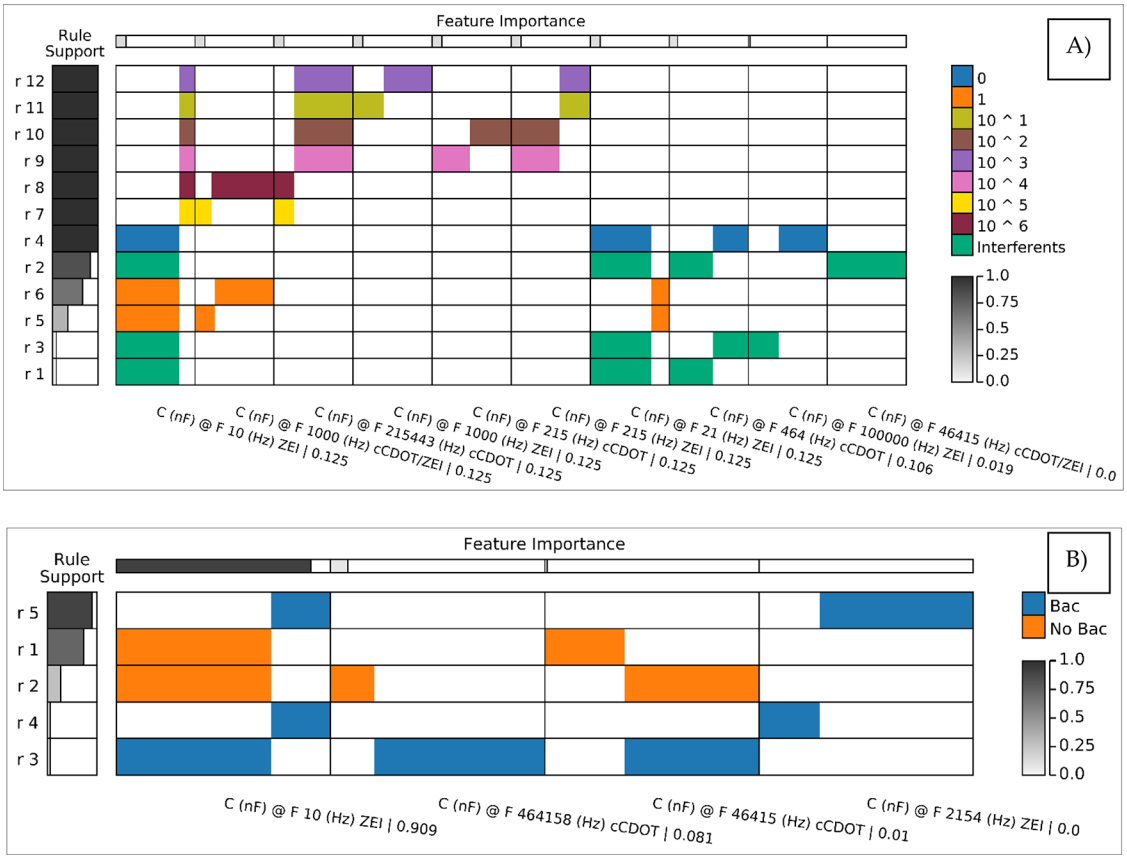

Figure 6. (A) Multidimensional Calibration Space (MCS) for the e-tongue in a multiclass scenario (9 classes). The classes are the 8 discretized *S. aureus* concentrations (1, 10, 10^2, 10^3, 10^4, 10^5, and 10^6 CFU/mL) and another grouping the 5 possible interferents, namely, glucose (GLU), lactose (LAC), urea (URE), mucin (MUC), and *Salmonella* (SAL). The MCS has 10 dimensions corresponding to 10 frequencies (features) selected among the 57 available (1 to 10^6 Hz for 3 sensor architectures). Frequencies from all 3 architectures are used, and the most important is 10 Hz from ZEI. Rules with maximum support are rules r4, r11, r10, r12, r9, r7, and r8 (first to the seventh row), distinguishing all samples from concentrations 0 (blue), 10 (olive), 10^2 (brown), 10^3 (purple), 10^4 (pink), 10^5 (yellow), and 10^6 (maroon) CFU/mL. The classification of 1 CFU/mL (orange) and the interferents (emerald) requires the low support rules r5, r3, and r1 (last three rows). The average accuracy estimated for the MCS is 86.1%; (b) Multidimensional Calibration Space (MCS) for the e-tongue in a binary classification, with classes "Bac" (bacteria presence) comprising data for *S. aureus* samples with concentrations 1, 10, 10^2, $10,^3$ $10,^4$ 10^5, and 10^6 CFU/mL, and "No Bac" (bacteria absence). The latter comprise data from 5 interferents (glucose (GLU), lactose (LAC), urea (URE), mucin (MUC), and *Salmonella*). The MCS has 4 dimensions corresponding to 4 frequencies (features) selected among the 57 available (1 to 106 Hz for 3 sensor architectures). Frequencies from ZEI and cCDOT architectures are used, while cCDOT/ZEI is not needed. The most important feature is 10 Hz from ZEI. Low support rules for both classes (Bac and No Bac) are required, viz., r2, r4, and r3 (last three rows). The average accuracy estimated for the MCS is 88.8%.

work with electronic tongues is the device calibration, in addition to verify selectivity for the task being performed. Because the problems addressed with electronic tongues normally do not involve a single analyte, unlike most of the work in analytical chemistry, calibration curves cannot be obtained. This gap can be filled using the concept of multidimensional calibration space (MCS),[29] in which supervised machine learning methods based on decision trees or random forests[35−37] are employed to explain how samples are classified. We have obtained an MCS from the capacitance spectra of milk samples spiked with *S. aureus* (1, 10, $10,^2$ $10,^3$ $10,^4$ 10^5, and 10^6 CFU/mL) and the interferents glucose (GLU), lactose (LAC), urea (URE), mucin (MUC), and *Salmonella* (SAL). The corresponding MCS is represented in Figure 6A where concentrations were discretized as classes, and all types of interferents were grouped as class "Interferents". It is thus a multiclass problem,[35,36] in this case with 9 classes. The 10-dimension MCS obtained with DT models and the Nested KFold Cross-Validation procedure (with k_outer = 3 and k_inner = 2)[39,40] for determining the hyperparameters and estimating performance had an average accuracy of 86.1%. Its visual representation in Figure 6A was generated with the ExMatrix method[38] using visualization with logic rules as rows, features as columns, and rule predicates as cells. The latter delimits range values (rectangular shapes) of capacitance to separate classes (e.g., bacteria concentrations) mapped as colors. The 10 dimensions (features) correspond to 10 frequencies selected among the 57 frequencies in the spectra (19 frequencies for each of the 3 sensing units). Note that frequencies from all 3 sensor architectures are used, the most important one being 10 Hz for the measurements with the ZEI sensing unit (first column), with an importance value of 0.125. The concentrations 0 (blue), 10 (olive), 10^2 (brown), 10^3 (purple), 10^4 (pink), 10^5 (yellow), and 10^6 (maroon) CFU/mL are easily mapped by generic rules (r4, r11, r10, r12, r9, r7, and r8). In contrast, the concentration 1 CFU/mL (orange) and the interferents samples (emerald) are more difficult to classify, requiring low support rules (r5, r3, and r1 at the last three rows).

https://doi.org/10.1021/acsomega.2c07944
ACS Omega 2023, 8, 13721−13732

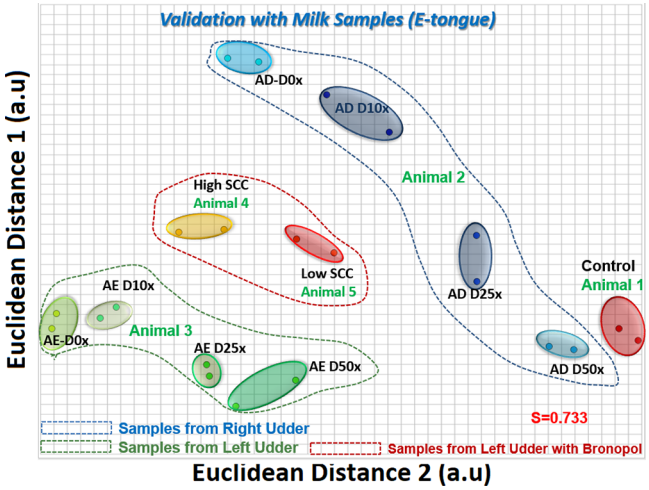

Figure 7. IDMAP projection of the capacitance spectra of e-tongue made with three sensors (cCDOT/ZEI, cCDOT, and ZEI) obtained in crude milk from cows. Also included are data from milk of a healthy cow (Control).

Similar procedures were used to obtain the 4-dimension MCS in Figure 6B for the binary classification where the milk samples containing *S. aureus* were grouped as class "Bac" (bacteria presence) and the interferents were grouped as "No Bac" (bacteria absence). The accuracy in the binary classification was 88.8%. Two of the 4 features selected originated from the spectra with the ZEI sensing unit (10 and 2154 Hz - first and last columns) while the other 2 came from cCDot (464,158 and 46,415 Hz - second and third columns). Thus, no frequencies from the cCDOT/ZEI architecture are needed for this calibration. Moreover, the most important feature is 10 Hz for ZEI (first column), with an importance value of 0.909. Low support rules are needed in both "Bac" (bacteria presence) and "No Bac" (bacteria absence) classes, also revealing a separability complexity for the binary problem.

3.4. Validation with Milk Samples from Animals Naturally Infected with Mastitis. The electronic tongue was used to detect *S. aureus* in crude milk samples collected from animals naturally infected with mastitis, in addition to milk for a healthy cow, used as control. Capacitance spectra were obtained with milk from five (5) different dairy cows (4 naturally infected with mastitis and 1 healthy cow), with the samples categorized into 11 classes, as specified in Section 2.2. Figure 7 shows an IDMAP projection for the eleven classes. Milk samples from the right udder indicate a lower *S. aureus* concentration than those from the left udder, with the clusters close to the control samples (sample 1). Diluted milk samples (3, 4, 5, 7, 8, 9) have electrical characteristics closer to the control sample, indicating a lower concentration of *S. aureus* per volume compared to undiluted samples (samples 2 and 6). The samples with greater dilution (samples 5 and 9) are closer to the control sample. Samples 10 and 11 treated with bronopol did not have *S. aureus* but could be distinguished from the control samples and samples with *S. aureus* owing to their somatic cells. The silhouette coefficient was 0.733, indicating an excellent distinction power. This performance is due to the electrical combination of responses from the three sensing units, whose molecular architectures had a high distinguish power, competitive with Soares et al.[18] The silhouette coefficients were 0.648, 0.588, and 0.643 for cCDOT/ZEI, cCDOT, and ZEI, respectively (Figure S4-A, S4-B, and S4-C in the Supporting Information).

In addition to classifying the eleven classes with IDMAP, an MCS was created with the capacitance spectra.[29] Figure 8 shows the representation of the 5-dimension MCS for the samples from 5 animals (4 cows naturally infected with mastitis and 1 healthy cow); the accuracy was 80.1%, with Nested KFold Cross-Validation with k_outer = 3 and k_inner = 2. The most important feature for classification was 4 Hz for the capacitance measurement with the cCDOT sensing unit, whose importance value was 0.250.

4. MECHANISMS BEHIND DETECTION

Electronic tongues are based on a global selectivity concept, in which non-specific interactions govern the detection mechanism. To investigate the interaction between *S. aureus* and the three molecular architectures in the sensing units, we employed polarization-modulated infrared reflection-absorption spectroscopy (PM-IRRAS). The PM-IRRAS spectra were taken from the reflectivity of the parallel (p) and perpendicular (s) components of the light incidence plane. Hence, one may

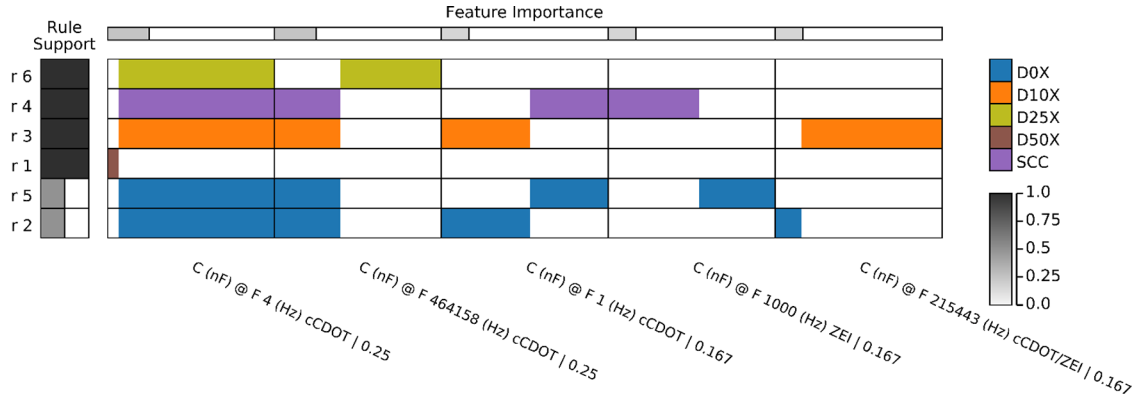

Figure 8. Multidimensional Calibration Space (MCS) for the e-tongue in a multiclass scenario (5 classes). The classes are milk samples from four (4) different animals infected with mastitis, providing samples with low and high SCC concentration and infected milk samples diluted 0, 10, 25, and 50×. The MCS has 5 dimensions corresponding to 5 frequencies (features) selected among the 57 available (1 to 10^6 Hz for 3 sensor architectures). Frequencies from all 3 architectures are used, and the most important is 4 Hz from cCDOT. Rules with maximum support are found, as for rules r6, r4, r3, and r1. The average accuracy estimated for the MCS via the DT model is 80.1%.

https://doi.org/10.1021/acsomega.2c07944
ACS Omega 2023, 8, 13721−13732

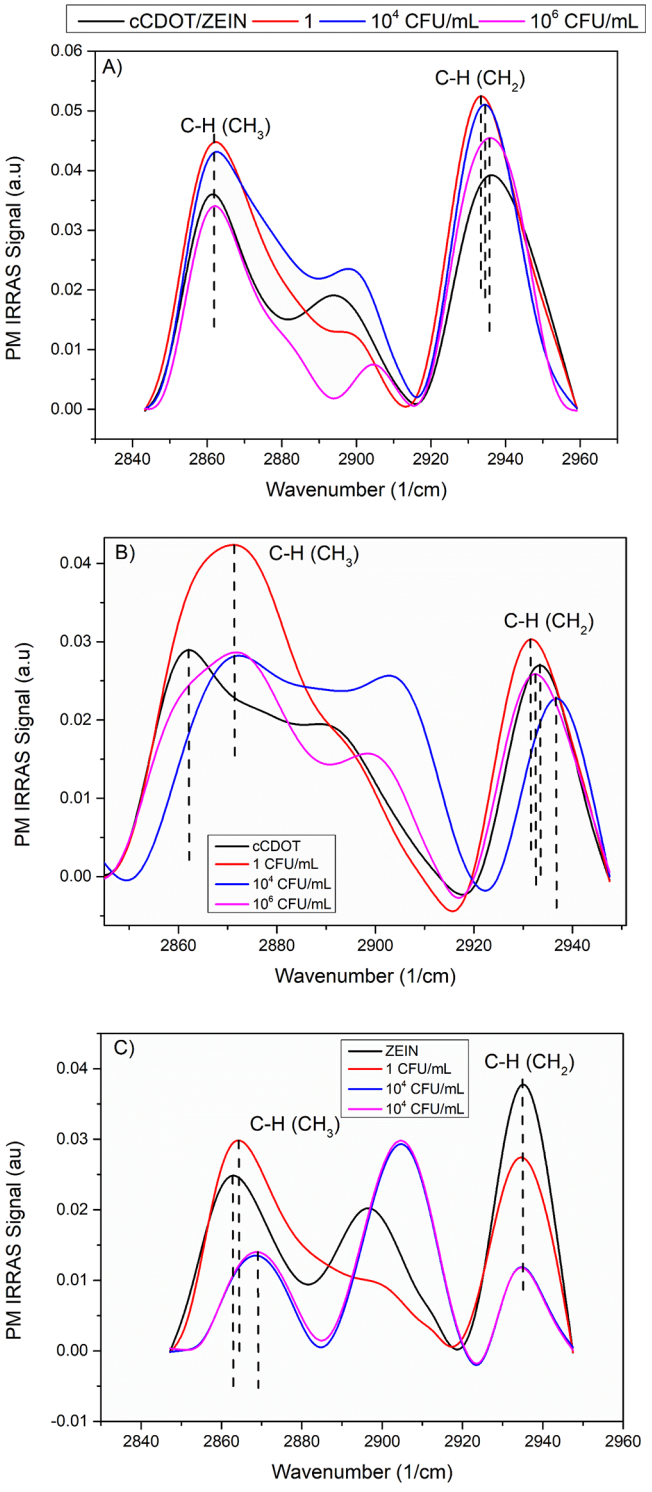

Figure 9. Normalized PM-IRRAS spectra for the e-tongue made from non-specific adsorption between *S. aureus* with (A) cCDOT/ZEI, (B) cCDOT, and (C) ZEI. The baseline was taken as the spectrum for each film before exposure to the milk samples containing *S. aureus*. Please see Table S2 in the Supporting Information for PM-IRRAS signal values for each *S. aureus* concentrations.

infer the changes in molecular orientation.[46,47] The signal was taken by eq 5.

$$\frac{\Delta R}{R} = \frac{Rp - Rs}{Rp + Rs} \quad (5)$$

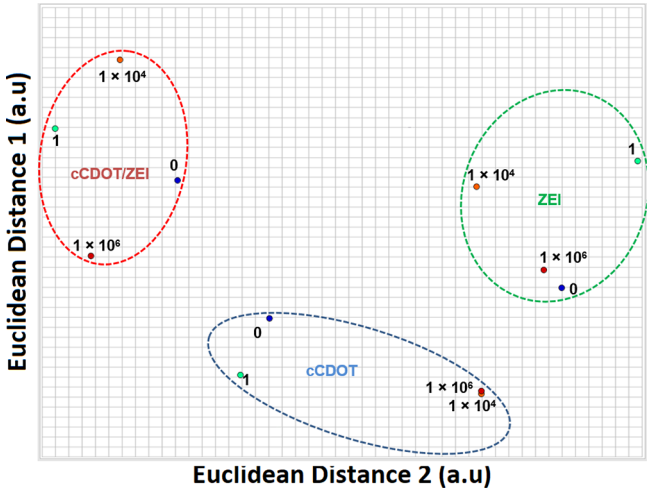

Figure 10. IDMAP projection of the PM-IRRAS spectra for cCDOT/ZEI, cCDOT, and ZEI films in detecting *S. aureus* in milk samples.

Figure 9 shows the normalized (see the raw spectra in Figure S5 of the Supporting Information) spectra for the molecular architectures deposited on gold substrates, before and after exposure to blank milk contaminated with three *S. aureus* concentrations (1, 1 × 10^4, and 1 × 10^6 CFU/mL). Characteristic bands due to adsorption of *S. aureus* are observed at 2860−2870 and 2933−2938 cm^{-1}, assigned to υC−H from CH_3 and CH_2, respectively.[48−52] Due to the polarization modulation in PM-IRRAS,[46,53] changes in the intensity/band area can be associated with either adsorption/desorption of materials or changes in orientation of the molecular dipoles.[46,53−55] The non-monotonic changes in intensity/area of the CH_3 band with *S. aureus* concentration indicate the orientation of υC−H dipole changes with non-specific interactions with cCDOT/ZEI, cCDOT, and ZEI films. The same applies to the CH_2 bands, except for the ZEI film in Figure 7C. Hence, the non-specific interactions between *S. aureus* and ZEI do not change the υC-H dipole orientation, probably owing to a higher molecular organization of ZEI.

The changes in the PM-IRRAS spectra in Figure 9 do indicate that the molecular-level interactions between *S. aureus* and the sensing units can be captured, which explains the high sensitivity in the impedance spectroscopy measurements. Because the changes are not monotonic with the *S. aureus* concentrations, we treated the whole PM-IRRAS spectra with IDMAP, whose projection is shown in Figure 10. Two aspects are worth mentioning from a visual inspection. First, as expected from the electrical measurements, the milk samples with different *S. aureus* concentrations are distinguishable. On the other hand, judging only by the IDMAP plot the sensing unit made with the ZEI architecture seems to be less adequate for distinguishing among the *S. aureus* samples, in contrast to the expectation from the electrical impedance spectroscopy data. This discrepancy is explained by the lack of change in the dipole orientation of the CH_2 groups, which only occurred for the ZEI architecture. For this lack of orientation, change decreases the differences in the overall PM-IRRAS spectra but makes it easier to distinguish the different *S. aureus* concentrations through the intensity of the CH_2 bands.

https://doi.org/10.1021/acsomega.2c07944
ACS Omega 2023, 8, 13721−13732

5. CONCLUSIONS

We have shown that flexible sensors can be used in a nanoarchitectonic electronic tongue to detect *S. aureus* in milk, which amounts to diagnosing bovine mastitis. This was actually demonstrated by distinguishing milk samples from mastitis-infected cows from milk collected from healthy cows. Even when used separately, the sensing units already had high sensitivity in detecting *S. aureus*. Indeed, the limits of detection (LoD) were 1.74, 4.19, and 0.83 CFU/mL for the three sensing units, namely, cCDOT/ZEI, cCDOT, and ZEI, respectively, with no false positives. These values are competitive with the devices in the literature[8−17,54,56] with the advantage of having sensing units that do not require specific interactions with a given analyte. This reduces fabrication costs, especially compared to biosensors. With the global selectivity concept, the electrical properties of distinct sensing units combined provide a pattern that is unique for a liquid sample. Thus, this electronic tongue has a diagnostic time of approximately 1 min for each molecular architecture (3 min in total), confirming its effectiveness in rapid diagnosis. The higher performance of the zein-containing sensing unit (ZEI) was attributed to some specificity in the interaction between zein and molecular groups in *S. aureus*. In addition to processing the impedance spectroscopy data with IDMAP, thus confirming the distinguishability of the milk samples, we obtained multidimensional calibration spaces (MCS) upon employing machine learning based on decision trees algorithms. The availability of low cost electronic tongues with impedance measurements that can be made with portable instruments may be transformative in diagnosing mastitis and other diseases in the farms, with no need of specialized laboratories.

■ ASSOCIATED CONTENT

Supporting Information

The Supporting Information is available free of charge at https://pubs.acs.org/doi/10.1021/acsomega.2c07944.

Electrical *S. aureus* detection (e.g., interferent test, complementary IDMAP plots data), mechanism behind detection (raw data from PM IRRAS), and electrode mask (PDF)

■ AUTHOR INFORMATION

Corresponding Authors

Osvaldo N. Oliveira, Jr − *São Carlos Institute of Physics (IFSC), University of São Paulo (USP), São Carlos 13566-590, Brazil;* orcid.org/0000-0002-5399-5860; Email: chu@ifsc.usp.br

Luiz Henrique Capparelli Mattoso − *Nanotechnology National Laboratory for Agriculture (LNNA), Embrapa Instrumentação, São Carlos 13560-970, Brazil;* orcid.org/0000-0001-7586-1014; Email: luiz.mattoso@embrapa,br

Authors

Andrey Coatrini Soares − *Nanotechnology National Laboratory for Agriculture (LNNA), Embrapa Instrumentação, São Carlos 13560-970, Brazil;* orcid.org/0000-0003-4601-3555

Juliana Coatrini Soares − *São Carlos Institute of Physics (IFSC), University of São Paulo (USP), São Carlos 13566-590, Brazil;* orcid.org/0000-0001-5455-1770

Danilo Martins dos Santos − *Nanotechnology National Laboratory for Agriculture (LNNA), Embrapa Instrumentação, São Carlos 13560-970, Brazil;* orcid.org/0000-0002-3884-3236

Fernanda L. Migliorini − *Nanotechnology National Laboratory for Agriculture (LNNA), Embrapa Instrumentação, São Carlos 13560-970, Brazil;* orcid.org/0000-0002-9605-2790

Mario Popolin-Neto − *Federal Institute of São Paulo (IFSP), Araraquara 14804-296, Brazil*

Danielle dos Santos Cinelli Pinto − *Embrapa Gado de Leite CEP, Juiz de Fora 3603-330, Brazil; Programa de Pós-Graduação em Ciências Veterinárias, Federal University of Lavras (UFLA), Lavras 37200-900, Brazil*

Wanessa Araújo Carvalho − *Embrapa Gado de Leite CEP, Juiz de Fora 3603-330, Brazil*

Humberto Mello Brandão − *Embrapa Gado de Leite CEP, Juiz de Fora 3603-330, Brazil; Programa de Pós-Graduação em Ciências Veterinárias, Federal University of Lavras (UFLA), Lavras 37200-900, Brazil*

Fernando Vieira Paulovich − *Department of Mathematics and Computer Science, Eindhoven University of Technology (TU/e), Eindhoven 5600 MB, the Netherlands*

Daniel Souza Correa − *Nanotechnology National Laboratory for Agriculture (LNNA), Embrapa Instrumentação, São Carlos 13560-970, Brazil*

Complete contact information is available at: https://pubs.acs.org/10.1021/acsomega.2c07944

Author Contributions

[▽]A.C.S. and J.C.S. contributed equally to this work. A.C.S.: conceptualization; data curation; formal analysis; investigation; methodology; project administration; writing − review & editing (responsible for performing experiments, data analysis, preparing the figures, and writing the manuscript); J.C.S.: formal analysis; investigation; methodology; writing − review & editing (responsible for carrying out the statistical analysis with information visualization techniques and analyzing the corresponding data and PM IRRAS measurements); D.M.d.S.: formal analysis; investigation; methodology; writing − review & editing (performed the electrode preparation and characterization); F.L.M.: formal analysis; investigation; methodology; writing − review & editing (performed the electrode preparation and characterization); M.P.-N.: formal analysis; investigation; methodology; writing − review & editing (performed the machine learning experiments at Federal Institute of São Paulo); D.d.S.C.P.: formal analysis; investigation; methodology; writing − review & editing (performed the extraction and analysis of crude milk characteristics at Embrapa Gado de Leite and Federal University of Lavras); W.A.C.: formal analysis; investigation; methodology; project administration; writing − review & editing (responsible for the experiments and data analysis at Embrapa Gado de Leite); H.M.B.: formal analysis; investigation; methodology; supervision; funding acquisition; padministration; writing − review & editing (responsible for the experiments and data analysis at Embrapa Gado de Leite); F.V.P.: formal analysis; investigation; methodology; supervision; project administration; writing − review & editing (responsible for the experiments and data analysis at Eindhoven University of Technology); D.S.C.: formal analysis; investigation; methodology; supervision; project administration; writing − review & editing (responsible

https://doi.org/10.1021/acsomega.2c07944
ACS Omega 2023, 8, 13721−13732

for the experiments and data analysis at Embrapa Instrumentação); O.N.O.: formal analysis; investigation; methodology; supervision; funding acquisition; project administration; writing − review & editing (responsible for the experiments and data analysis at IFSC-USP and was the research co-coordinator and edited the manuscript); L.H.C.M.: formal analysis; investigation; methodology; supervision; funding acquisition; project administration; writing − review & editing (was the research coordinator and edited the manuscript). All authors have read and agreed to the published version of the manuscript.

Notes

The authors declare no competing financial interest.

■ ACKNOWLEDGMENTS

This work was supported by São Paulo Research Foundation (FAPESP) (Grant numbers: 2018/ 18953-8, 2018/22214-6, 2017/21791-7, 2017/20973-4, 2017/121-74-4), FAPEMIG (CVZ PPM 00691/17 and RED-00282/16), CNPq, SISNANO-MCTI, the Financier of Studies and Projects (FINEP), INEO and Rede Agronano/Embrapa. The authors thank Joana Bresolin (Embrapa Instrumentação), Debora T. Balogh (São Carlos Institute of Physics), Prof. Paulo Machado (ESALQ-USP/ Clínica do Leite), and Mr. Augusto Lima (Clínica do Leite).

■ REFERENCES

(1) Cheng, W. N.; Han, S. G. Bovine Mastitis: Risk Factors, Therapeutic Strategies, and Alternative Treatments — A Review. *Asian-Australas J. Anim. Sci.* **2020**, *33*, 1699−1713.

(2) Monistero, V.; Graber, H.; Pollera, C.; Cremonesi, P.; Castiglioni, B.; Bottini, E.; Ceballos-Marquez, A.; Lasso-Rojas, L.; Kroemker, V.; Wente, N.; Petzer, I.-M.; Santisteban, C.; Runyan, J.; Veiga dos Santos, M.; Alves, B.; Piccinini, R.; Bronzo, V.; Abbassi, M.; Said, M.; Moroni, P. Staphylococcus Aureus Isolates from Bovine Mastitis in Eight Countries: Genotypes, Detection of Genes Encoding Different Toxins and Other Virulence Genes. *Toxins* **2018**, *10*, 247.

(3) Viguier, C.; Arora, S.; Gilmartin, N.; Welbeck, K.; O'Kennedy, R. Mastitis Detection: Current Trends and Future Perspectives. *Trends Biotechnol.* **2009**, *27*, 486−493.

(4) Martins, S. A. M.; Martins, V. C.; Cardoso, F. A.; Germano, J.; Rodrigues, M.; Duarte, C.; Bexiga, R.; Cardoso, S.; Freitas, P. P. Biosensors for On-Farm Diagnosis of Mastitis. *Front. Bioeng. Biotechnol.* **2019**, *7*, 186.

(5) Antanaitis, R.; Juozaitienė, V.; Jonike, V.; Baumgartner, W.; Paulauskas, A. Milk Lactose as a Biomarker of Subclinical Mastitis in Dairy Cows. *Animals* **2021**, *11*, 1736.

(6) Oliver, S. P.; Lewis, M. J.; Gillespie, B. E.; Downlen, H. H.; Jaenicke, E.; Roberts, R. K. *Microbiological Procedures for the Diagnosis of Bovine Udder Infection and Determination of Milk Quality*, 4th ed.; National Mastitis Council: Verona, 2004.

(7) Ashraf, A.; Imran, M. Diagnosis of Bovine Mastitis: From Laboratory to Farm. *Trop Anim Health Prod* **2018**, *50*, 1193−1202.

(8) Juronen, D.; Kuusk, A.; Kivirand, K.; Rinken, A.; Rinken, T. Immunosensing System for Rapid Multiplex Detection of Mastitis-Causing Pathogens in Milk. *Talanta* **2018**, *178*, 949−954.

(9) Peedel, D.; Rinken, T. Rapid Biosensing of Staphylococcus Aureus Bacteria in Milk. *Anal. Methods* **2014**, *6*, 2642.

(10) Jia, F.; Duan, N.; Wu, S.; Ma, X.; Xia, Y.; Wang, Z.; Wei, X. Impedimetric Aptasensor for Staphylococcus Aureus Based on Nanocomposite Prepared from Reduced Graphene Oxide and Gold Nanoparticles. *Microchim. Acta* **2014**, *181*, 967−974.

(11) Wang, H.; Xiu, Y.; Chen, Y.; Sun, L.; Yang, L.; Chen, H.; Niu, X. Electrochemical Immunosensor Based on an Antibody-Hierarchical Mesoporous SiO_2 for the Detection of *Staphylococcus Aureus*. *RSC Adv.* **2019**, *9*, 16278−16287.

(12) Wilson, D.; Materón, E. M.; Ibáñez-Redín, G.; Faria, R. C.; Correa, D. S.; Oliveira, O. N. Electrical Detection of Pathogenic Bacteria in Food Samples Using Information Visualization Methods with a Sensor Based on Magnetic Nanoparticles Functionalized with Antimicrobial Peptides. *Talanta* **2019**, *194*, 611−618.

(13) Idil, N.; Bakhshpour, M.; Perçin, I.; Mattiasson, B. Whole Cell Recognition of Staphylococcus Aureus Using Biomimetic SPR Sensors. *Biosensors* **2021**, *11*, 140.

(14) Cui, J.; Zhou, M.; Li, Y.; Liang, Z.; Li, Y.; Yu, L.; Liu, Y.; Liang, Y.; Chen, L.; Yang, C. A New Optical Fiber Probe-Based Quantum Dots Immunofluorescence Biosensors in the Detection of Staphylococcus Aureus. *Front. Cell. Infect. Microbiol.* **2021**, *11*, 665241.

(15) Cai, R.; Zhang, Z.; Chen, H.; Tian, Y.; Zhou, N. A Versatile Signal-on Electrochemical Biosensor for Staphylococcus Aureus Based on Triple-Helix Molecular Switch. *Sens. Actuators, B* **2021**, *326*, 128842.

(16) Zelada-Guillén, G. A.; Sebastián-Avila, J. L.; Blondeau, P.; Riu, J.; Rius, F. X. Label-Free Detection of Staphylococcus Aureus in Skin Using Real-Time Potentiometric Biosensors Based on Carbon Nanotubes and Aptamers. *Biosens. Bioelectron.* **2012**, *31*, 226−232.

(17) Lee, C.-W.; Chang, H.-Y.; Wu, J.-K.; Tseng, F.-G. Ultra-Sensitive Electrochemical Detection of Bacteremia Enabled by Redox-Active Gold Nanoparticles (RaGNPs) in a Nano-Sieving Microfluidic System (NS-MFS). *Biosens. Bioelectron.* **2019**, *133*, 215−222.

(18) Coatrini Soares, A.; Coatrini Soares, J.; Popolin-Neto, M.; Scarpa de Mello, S.; Dos Santos Cinelli Pinto, D.; Araújo Carvalho, W.; Gilmore, M. S.; Helena Oliveira Piazzetta, M.; Luiz Gobbi, A.; de Melo Brandão, H.; Vieira Paulovich, F.; Oliveira, O. N.; Henrique Capparelli Mattoso, L. Microfluidic E-Tongue To Diagnose Bovine Mastitis with Milk Samples Using Machine Learning with Decision Tree Models. *Chem. Eng. J.* **2022**, 138523.

(19) Toko, K. A Taste Sensor. *Meas. Sci. Technol.* **1998**, *9*, 1919−1936.

(20) Riul, A.; dos Santos, D. S.; Wohnrath, K.; Di Tommazo, R.; Carvalho, A. C. P. L. F.; Fonseca, F. J.; Oliveira, O. N.; Taylor, D. M.; Mattoso, L. H. C. Artificial Taste Sensor: Efficient Combination of Sensors Made from Langmuir−Blodgett Films of Conducting Polymers and a Ruthenium Complex and Self-Assembled Films of an Azobenzene-Containing Polymer. *Langmuir* **2002**, *18*, 239−245.

(21) Di Rosa, A. R.; Leone, F.; Chiofalo, V. Electronic Noses and Tongues. *In Chemical Analysis of Food;* Elsevier, 2020; pp. 353−389. DOI: 10.1016/B978-0-12-813266-1.00007-3.

(22) Facure, M. H. M.; Braunger, M. L.; Mercante, L. A.; Paterno, L. G.; Riul, A.; Correa, D. S. Electrical Impedance-Based Electronic Tongues: Principles, Sensing Materials, Fabrication Techniques and Applications. In *Reference Module in Biomedical Sciences*; Elsevier, 2021; p B9780128225486000000. DOI: 10.1016/B978-0-12-822548-6.00091-1.

(23) Bonanni, A.; del Valle, M. Use of Nanomaterials for Impedimetric DNA Sensors: A Review. *Anal. Chim. Acta* **2010**, *678*, 7−17.

(24) Riul, A., Jr.; Dantas, C. A. R.; Miyazaki, C. M.; Oliveira, O. N., Jr. Recent Advances in Electronic Tongues. *Analyst* **2010**, *135*, 2481.

(25) Ghrissi, H.; Veloso, A. C. A.; Marx, Í. M. G.; Dias, T.; Peres, A. M. A Potentiometric Electronic Tongue as a Discrimination Tool of Water-Food Indicator/Contamination Bacteria. *Chemosensors* **2021**, *9*, 143.

(26) Kirsanov, D.; Korepanov, A.; Dorovenko, D.; Legin, E.; Legin, A. Indirect Monitoring of Protein A Biosynthesis in E.Coli Using Potentiometric Multisensor System. *Sens. Actuators, B* **2017**, *238*, 1159−1164.

(27) Minghim, R.; Paulovich, F. V.; de Andrade Lopes, A. Content-Based Text Mapping Using Multi-Dimensional Projections for Exploration of Document Collections; Erbacher, R. F.; Roberts, J. C.; Gröhn, M. T.; Börner, K., Eds.; SPIE San Jose, CA, 2006; p 60600S. DOI: 10.1117/12.650880.

(28) Paulovich, F. V.; Moraes, M. L.; Maki, R. M.; Ferreira, M.; Oliveira, O. N., Jr.; de Oliveira, M. C. F. Information Visualization Techniques for Sensing and Biosensing. *Analyst* **2011**, *136*, 1344.

https://doi.org/10.1021/acsomega.2c07944
ACS Omega 2023, 8, 13721−13732

(29) Neto, M. P.; Soares, A. C.; Oliveira, O. N.; Paulovich, F. V. Machine Learning Used to Create a Multidimensional Calibration Space for Sensing and Biosensing Data. *BCSJ* **2021**, *94*, 1553−1562.
(30) Ting, D.; Dong, N.; Fang, L.; Lu, J.; Bi, J.; Xiao, S.; Han, H. Multisite Inhibitors for Enteric Coronavirus: Antiviral Cationic Carbon Dots Based on Curcumin. *ACS Appl. Nano Mater.* **2018**, *1*, 5451−5459.
(31) Dos Santos, D. M.; Migliorini, F. L.; Soares, A. C.; Mattoso, L. H. C.; Oliveira, O. N.; Correa, D. S. Electrochemical Immunosensor Made with Zein-based Nanofibers for On-site Detection of Aflatoxin B1. *Electroanalysis* **2023**, elan.202100672.
(32) Soares, J. C.; Soares, A. C.; Rodrigues, V. D. C.; Oiticica, P. R. A.; Raymundo-Pereira, P. A.; Bott-Neto, J. L.; Buscaglia, L. A.; Castro, L.; Ribas, L. C.; Scabini, L.; Brazaca, L. C.; Correa, D.; Mattoso, L. H.; Ferreira de Oliveira, M. C.; de Carvalho, A. C. P. L. F.; Carrilho, E.; Bruno, O. M.; Melendez, M. E.; Novais Oliveira, O., Jr. Detection of a SARS-CoV-2 Sequence with Genosensors Using Data Analysis Based on Information Visualization and Machine Learning Techniques. *Mater. Chem. Front.* **2021**, 5658.
(33) Inselberg, A.; Dimsdale, B. Parallel Coordinates: A Tool for Visualizing Multi-Dimensional eGeometry. In *Proceedings of the First IEEE Conference on Visualization: Visualization 90*; IEEE Comput. Soc. Press: San Francisco, CA, USA, 1990; pp. 361−378. DOI: 10.1109/VISUAL.1990.146402.
(34) Soares, J. C.; Shimizu, F. M.; Soares, A. C.; Caseli, L.; Ferreira, J.; Oliveira, O. N. Supramolecular Control in Nanostructured Film Architectures for Detecting Breast Cancer. *ACS Appl. Mater. Interfaces* **2015**, *7*, 11833−11841.
(35) Tan, P.-N.; Steinbach, M.; Kumar, V. *Introduction to Data Mining*, 1st ed.; Pearson Addison Wesley: Boston, 2006.
(36) James, G.; Witten, D.; Hastie, T.; Tibshirani, R. *An Introduction to Statistical Learning*; Springer Texts in Statistics; Springer New York: New York, NY, 2013; Vol. *103*. DOI: 10.1007/978-1-4614-7138-7.
(37) *Classification and Regression Trees*, 1. CRC Press repr.; Breiman, L., Ed.; Chapman & Hall/CRC: Boca Raton, Fla., 1998.
(38) Neto, M. P.; Paulovich, F. V. Explainable Matrix - Visualization for Global and Local Interpretability of Random Forest Classification Ensembles. *IEEE Trans. Visual. Comput. Graphics* **2021**, *27*, 1427−1437.
(39) Varma, S.; Simon, R. Bias in Error Estimation When Using Cross-Validation for Model Selection. *BMC Bioinformatics* **2006**, *7*, 91.
(40) Tsamardinos, I.; Rakhshani, A.; Lagani, V. Performance-Estimation Properties of Cross-Validation-Based Protocols with Simultaneous Hyper-Parameter Optimization. In *Artificial Intelligence: Methods and Applications*; Likas, A.; Blekas, K.; Kalles, D., Eds.; Hutchison, D.; Kanade, T.; Kittler, J.; Kleinberg, J. M.; Kobsa, A.; Mattern, F.; Mitchell, J. C.; Naor, M.; Nierstrasz, O.; Pandu Rangan, C.; Steffen, B.; Terzopoulos, D.; Tygar, D.; Weikum, G., Series Eds.; Lecture Notes in Computer Science; Springer International Publishing: Cham, 2014; Vol. 8445, pp 1−14. DOI: 10.1007/978-3-319-07064-3_1.
(41) Barsoukov, E.; Macdonald, J. R. *Impedance Spectroscopy Theory, Experiment, and Applications.*; Wiley-Interscience: Hoboken, N.J., 2005.
(42) Lvovich, V. F. *Impedance Spectroscopy: Applications to Electrochemical and Dielectric Phenomena*; Wiley: Hoboken, N.J, 2012.
(43) Currie, L. A. Nomenclature in Evaluation of Analytical Methods Including Detection and Quantification Capabilities (IUPAC Recommendations 1995). *Pure Appl. Chem.* **1995**, *67*, 1699−1723.
(44) McKinnon, C. H.; Rowlands, G. J.; Bramley, A. J. The Effect of Udder Preparation before Milking and Contamination from the Milking Plant on Bacterial Numbers in Bulk Milk of Eight Dairy Herds. *J. Dairy Res.* **1990**, *57*, 307−318.
(45) Soares, A. C.; Soares, J. C.; Shimizu, F. M.; Melendez, M. E.; Carvalho, A. L.; Oliveira, O. N. Controlled Film Architectures to Detect a Biomarker for Pancreatic Cancer Using Impedance Spectroscopy. *ACS Appl. Mater. Interfaces* **2015**, *7*, 25930−25937.
(46) Greenler, R. G. Infrared Study of Adsorbed Molecules on Metal Surfaces by Reflection Techniques. *The Journal of Chemical Physics* **1966**, *44*, 310−315.
(47) Golden, W. A Method for Measuring Infrared Reflection? Absorption Spectra of Molecules Adsorbed on Low-Area Surfaces at Monolayer and Submonolayer Concentrations. *J. Catal.* **1981**, *71*, 395−404.
(48) Colthup, N. B.; Daly, L. H.; Wiberley, S. E. *Introduction to Infrared and Raman Spectroscopy*, 3rd ed.; Academic Press: Boston, 1990.
(49) Wieckowski, A.; Korzeniewski, C.; Braunschweig, B. *Vibrational Spectroscopy at Electrified Interfaces*; 2013.
(50) Barth, A. Infrared Spectroscopy of Proteins. *Biochimica et Biophysica Acta (BBA) - Bioenergetics* **2007**, *1767*, 1073−1101.
(51) Grunert, T.; Wenning, M.; Barbagelata, M. S.; Fricker, M.; Sordelli, D. O.; Buzzola, F. R.; Ehling-Schulz, M. Rapid and Reliable Identification of Staphylococcus Aureus Capsular Serotypes by Means of Artificial Neural Network-Assisted Fourier Transform Infrared Spectroscopy. *J. Clin. Microbiol.* **2013**, *51*, 2261−2266.
(52) Erukhimovitch, V.; Talyshinsky, M.; Souprun, Y.; Huleihel, M. Use of Fourier Transform Infrared Microscopy for the Evaluation of Drug Efficiency. *J. Biomed. Opt.* **2006**, *11*, No. 064009.
(53) Greenler, R. G. Design of a Reflection−Absorption Experiment for Studying the Ir Spectrum of Molecules Adsorbed on a Metal Surface. *J. Vac. Sci. Technol.* **1975**, *12*, 1410−1417.
(54) Soares, A. C.; Soares, J. C.; Rodrigues, V. C.; Oliveira, O. N.; Capparelli Mattoso, L. H. Controlled Molecular Architectures in Microfluidic Immunosensors for Detecting Staphylococcus Aureus. *Analyst* **2020**, *145*, 6014−6023.
(55) Soares, A. C.; Soares, J. C.; Rodrigues, V. C.; Follmann, H. D. M.; Arantes, L. M. R. B.; Carvalho, A. C.; Melendez, M. E.; Fregnani, J. H. T. G.; Reis, R. M.; Carvalho, A. L.; Oliveira, O. N. Microfluidic-Based Genosensor To Detect Human Papillomavirus (HPV16) for Head and Neck Cancer. *ACS Appl. Mater. Interfaces* **2018**, *10*, 36757−36763.
(56) Gu, Z.; Fu, A.; Ye, L.; Kuerban, K.; Wang, Y.; Cao, Z. Ultrasensitive Chemiluminescence Biosensor for Nuclease and Bacterial Determination Based on Hemin-Encapsulated Mesoporous Silica Nanoparticles. *ACS Sens.* **2019**, *4*, 2922−2929.

https://doi.org/10.1021/acsomega.2c07944
ACS Omega 2023, 8, 13721−13732